Fatigue and Fracture of Engineering Materials and Structures 2022, 1-15.
https://doi.org/10.1111/ffe.13890

On the use of milled shell-only specimens to study the effect of fibre orientation on the fatigue behaviour of a short fibre reinforced polyamide.

A. Canegrati[(a)], L.M. Martulli[(a)], P. Hine[(b)], C. Grassini[(c)], A. Bernasconi[(a,*)]

[(a)]Dipartimento di Meccanica, Politecnico di Milano, via La Masa 1, 20156 Milano, Italy

[(b)]Soft Matter Physics Research Group, School of Physics and Astronomy, University of Leeds, Leeds LS2 9JT, UK

[(c)]RadiciGroup High Performance Polymers, Chignolo d'Isola BG, Italy

Corresponding author: *, Dipartimento di Meccanica, Politecnico di Milano, via La Masa 1, 20156 Milano, Italy. Email: andrea.bernasconi@polimi.it

Abstract

The interpretation of the fibre orientation effects on the fatigue behaviour of short fibre reinforced polymers using specimens extracted from injection-moulded plates is hampered by the typical shell-core-shell structure, which affects the stress distribution through the sample's thickness. In this work, local fatigue strength values are obtained using specimens machined to leave only the outer shell layers, thus having a more homogeneous fibre orientation. Results of the finite element analysis of integer and shell-only specimens, accounting for locally measured fibre orientations, are compared. Conclusions are drawn about the role of the core layer and the limitations of milled specimens in the evaluation of the fatigue strength.

Keywords: Short fibre reinforced polymers, fatigue, fibre orientation, shell-only specimens, polyamide

Nomenclature

FCMA	Fiber Composite Material Analysis	a_{11}, a_{22}, a_{33}	Orientation tensor's components
FE	Finite Element	b	Fatigue strength exponent
FEA	Finite Element Analysis	F_{max}	Force that would lead the full specimens to failure at 10^6 loading cycles
FEM	Finite Element Method	N_f	Number of cycles to failure
FO	Fibre Orientation	R_a	Average surface roughness
FOD	Fibre Orientation Distribution	$\vartheta_x, \vartheta_y, \vartheta_z$	Angles between the fibre's axis and the *x*, *y* and *z* axes
OT	Orientation Tensor	σ_1	Stress component parallel to the principal direction of the orientation tensor

SEM	Scanning Electron Microscope	σ_2	Stress component perpendicular to the principal direction of the orientation tensor
SFRPs	Short Fibre Reinforced Polymers	σ_f'	Fatigue strength coefficient
TPM	Through Process Modelling	σ_{max}	Maximum nominal stress applied in a loading cycle
µCT	Micro-Computed Tomography	$\sigma_{max,10^6}$	Maximum nominal stress that would lead the specimens to failure at 10^6 cycles

1. Introduction

Fatigue of Short Fibre Reinforced Polymers (SFRPs) is a topic of growing interest, since these materials can be valid lightweight alternatives to metals. For a comprehensive review of the several factors affecting the fatigue of these materials, see [1]. Among them, anisotropy, the layered micro-structure often encountered in injection moulded parts and Fibre Orientation (FO) play a major role.

Anisotropy of SFRPs results from the manufacturing process, which in most cases is injection moulding. The melt polymer flowing into the mould already contains short fibres, which are transported by the flow throughout the mould cavity. Thus, the final fibre orientation distribution is the result of numerous complex phenomena related to the melt polymer flow dynamics. Several works dealt with the effect of anisotropy on the fatigue behaviour of SFRPs. Early works were based on the use of specimens extracted from edge injected, injection moulded plates, oriented at 0° and 90° from the mould flow direction [2], [3] and [4]. These works showed the presence of a shell-core-shell structure across the thickness of the plates. [5]. The mechanical and fatigue behaviour of SFRPs was found to be highly influenced by such layered microstructure [6-8].

In [9], the effect of fibre orientation on the fatigue behaviour of a polyamide 6 reinforced with 30% by weight of glass fibres (PA6GF30) was studied using specimens extracted from injection-moulded plates with different orientations (off-axis tests at 0°, 30°, 60° and 90°, with reference to the plate's longitudinal axis). The results were analysed in terms of the nominal stress, i.e. dividing the applied force by the area of the cross section. The shell-core-shell inner structure, and the consequent possible non-uniform stress distribution, due to non-uniform local stiffness through the specimen's thickness, were not considered. Using nominal stresses, a fatigue criterion derived from the Tsai-Hill criterion was proposed, which allowed the results of off-axis tests to be well fitted. Finally, a scaling method based on ultimate tensile strength values was proposed for relating

fatigue behaviour of specimens cut out from plates to standard ISO 527-2 type A specimens [10]. Using a similar approach but a shorter plate, De Monte et al. [11] obtained results in partial agreement with the experimental evidence of [9]: the effect of anisotropy was absent in the plates having 3 mm thickness, whereas off-axis specimens extracted from plates having 1 mm thickness displayed a similar trend as in [9]. Moreover, nominal stress results for 1 mm thick specimens fitted well with a Tsai-Hill relationship also in this case.

Through Process Modelling (TPM) was also used to tentatively predict and analyse the fatigue properties of SFRPs. TPM is based on the combination of process simulations and structural analyses. Overall, this approach allowed the application of multiaxial fatigue criteria on non-standard specimens, considering their layered orientation [12-14]. Alternatively, the resulting layered orientation from the injection moulding simulation can be averaged through the thickness: this was done by Launay et al. [15], who used a modified Tsai-Hill fatigue criterion [16]. Stadler et al. [17] also proposed a method in which the layered microstructure is neglected. The authors measured the fibre orientation distribution at specific locations of injection moulded plates. This allows fatigue models calibration with the strength values and the corresponding calculated fibre orientation at fracture locations.

Mortazavian and Fatemi [18] also successfully applied the Tsai-Hill criterion to fit off-axis fatigue strengths, expressed in terms of nominal stresses, for different orientations (i.e. 0°, 18°, 45° and 90°). In addition, the effect of specimen thickness was investigated using longitudinal and transverse specimens made of PA6GF35 tested at 23°C with a load ratio R=0.1. A small influence of thickness variation, ranging from 3.0 to 3.8 mm, was observed in the case of longitudinal specimens, while, in the case of transversal specimens, fatigue strength was significantly reduced going from 3.8 to 3.0 mm. It is worth noting that, as reported in [19] where similar specimens were used to characterize the effects of fibre orientation and anisotropy on tensile strength and elastic modulus of SFRPs, also the ratio of core thickness to the specimen thickness was different and equal to about 0.13 and 0.07 for the 3.8 and the 3 mm samples, respectively.

Finally, Jain et al. [20] raised criticism about the use of master S-N curves obtained by strength scaling and proposed new S-N master curves obtained using specimens cut from plates oriented at 0°, 45° and 90° with respect to the plate's axis. However, also in this case, the entire coupon was treated as a single representative volume element to whom a single fibre Orientation Tensor (OT) was associated. The same author in [21]

proposed two models for the prediction of the multi-axial fatigue behaviour of SFRC based on the master S-N curves approach, thence compatible with the through the process modelling framework. The limited data needed as input to the models could make them useful in designing phase of components made by SFRPs.

From this literature review, it appears that since the publication of [9], experimental and numerical analysis tools have evolved. TPM is becoming an industry standard. Process simulation nowadays is usually performed to predict the fibre orientation distribution over the whole part. Based on Fibre Orientation Distribution (FOD) obtained by process simulation, structural Finite Element (FE) analyses can be performed, allowing the evaluation of stresses on a local scale, thus gaining a more accurate view of the stress distributions. The fatigue strength of components can also be evaluated based on local stresses obtained with this approach, provided reliable local values of the fatigue strength depending on the local fibre orientation are available.

The measurement of such fatigue strengths, however, is challenging. Such criticality was highlighted in [22] and a possible solution was proposed. Some 0° and 90° specimens, belonging to the same batch of those used in [9] were machined to preserve only one shell layer of each specimen. Fatigue tests showed a mismatch between the fatigue response of the shell-only specimens and the integer multi-layered specimens [22]. It was thus suggested that, by excluding the contribution of the core layer, a more accurate estimation of the local fatigue strength can be obtained. However, the work of [22] was a preliminary investigation, affected by some uncertainties and a limited analysis. Namely, the water content between integer and the shell-only specimens was different.

In this work, the experimental procedure proposed in [22] is applied to a polyamide 6,6 reinforced with 50% glass fibres (PA66GF50). This is a more interesting material than PA6GF30 for load bearing applications, because of the higher strength and stiffness. Moreover, the higher fibre content resulted in a larger core thickness than in PA6GF30 samples. A comprehensive numerical analysis was performed to better understand the fatigue response of the integer and shell-only specimens. Overall, this work highlights an often-underestimated problem in the literature: the correct evaluation of the local fibre orientation-dependent fatigue strength of SFRPs to be used in TPM.

2. Experimental

2.1. Specimens manufacturing

The material investigated is a short glass fibre reinforced polyamide-66, with a E-glass content of 50% by weight (PA66 GF50). Rectangular plates, whose dimensions were 120 mm x 180 mm x 3.2 mm, were produced by injection moulding. Dog-bone specimens were water jet cut from the plates with orientations of 0° and 90° with respect to the plate's longitudinal axis, as illustrated in Figure 1.a. Their shape and dimensions are reported in Figure 1.b (being the plates 120 mm wide, specimens cut at 90° had a shorter total length of 116 mm, obtained by reducing the length of the grips only, without modifying the gauge length and the fillet radii).

In order to test the material close to the real service condition, the specimens underwent an accelerated conditioning (moisture absorption) prior to testing. The specimens were stored at 70°C and 70% relative humidity until the moisture absorption of the specimens had reached the equilibrium level. The weight of the specimens was monitored during the accelerated conditioning to ensure that equilibrium condition had been achieved.

Some specimens were then milled to preserve only one shell layer, as done in [22]. The 0° and 90° specimens were thus milled to a thickness of 0.8 mm, as identified by the FOD analysis reported in section 2.2. Milling was carried out in steps of 100 μm, with a final pass at a 10 μm depth to improve the surface finish. The milling machine was equipped with a carbide tipped, single edge fly cutting tool of 50 mm diameter. The rotational speed of the spindle was set to 2000 rpm, while the longitudinal cutting speed was limited to 1 mm/s.

In the rest of the work, the integer and the shell-only specimens will be referred to as "full specimens" and "milled specimens", respectively.

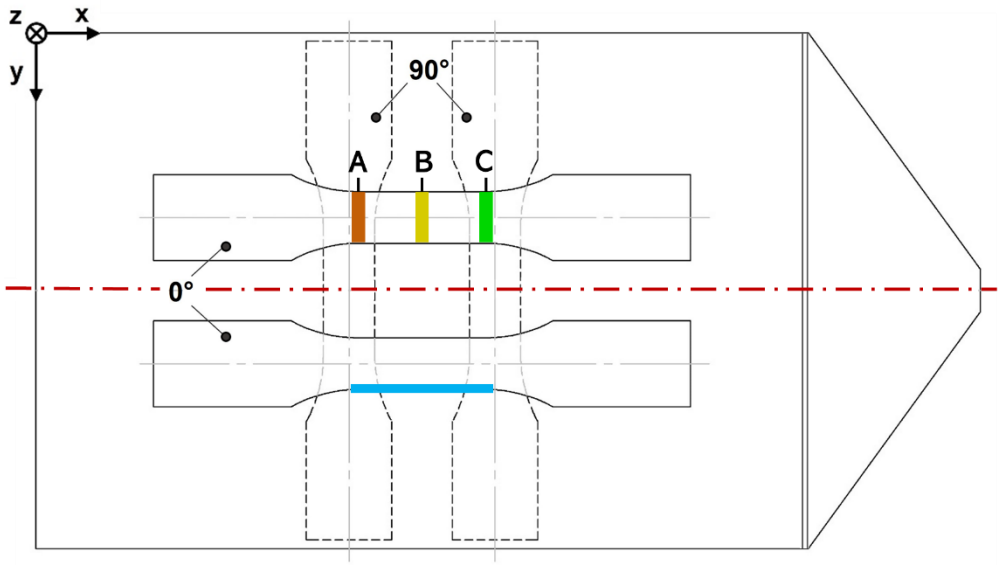

(a)

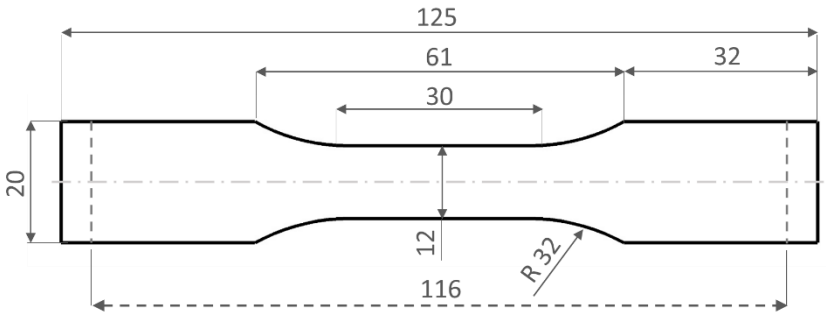

(b)

Figure 1. a) Location of the specimens in the injection moulded plates; the analysed surface for FOD measurements with ellipsometry is highlighted in light-blue and the positions of the µCT scanned samples are labelled as A, B, C and highlighted in red, yellow and green, respectively. b) Specimen shape and dimensions.

2.2 Testing conditions

Load controlled uniaxial fatigue tests were carried out on both the full and the milled specimens using an MTS servo-hydraulic uniaxial machine, with a 25 kN load cell. The load was applied sinusoidally at a constant minimum to maximum stress ratio of 0.1. The testing frequency was set to 4 Hz. Specimens' surface temperature was monitored during the tests through a resistance thermometer. The temperature increase due to the cyclic load was smaller than 4°C for all specimens, which is well below the 10°C maximum increase suggested by the standard [23]. The failure criterion adopted for fatigue test was specimen separation. If no separation occurred, the tests were interrupted at 10^6 number of cycles (run-outs).

Additional tensile tests were performed on the full specimens in order to evaluate their Young's moduli for both 0° and 90° orientations and use them to support the FE simulations. These latter tests were performed according to the ISO 527-2 [10], with a displacement rate of 5 mm/min. Both the tensile and the fatigue tests were run in a controlled environment. The temperature and the relative humidity were kept at 23°C±2°C and 50% ±5%, respectively.

2.3 Fibre orientation analysis

FOD was evaluated on the full specimens with two different methods: ellipsometry [24] and micro-Computed Tomography (µCT). Ellipsometry was used to analyse the lateral surface of the specimen's gauge length, highlighted in light blue in Figure 1.a. When a composite specimen is sectioned, the intersections between the sectioning plane and the fibres appear circular or elliptical. The measurement of the elliptical parameters of each fibre's footprint allows the determination of the angles that specify the 3D orientation of the fibre. In general, the 3D orientation of each fibre is fully described by only two angles, ϑ and φ [25]. Whitin the present framework, with reference to Figure 1, ϑ is defined as the angle between the fibre's axis and the z axis, while φ is the angle the projection of the fibre onto the x-y plane makes with the x axis. For the purpose of the present investigation, the 3D orientation of each single fibre within the analysed area is expressed in terms of ϑ_x, ϑ_y,and ϑ_z, namely the angles formed by the fibre's axis with the *x*, *y* and *z* axes (see Figure1), respectively. The analysed surface was split in to 33 equal strips parallel to the x axis. Fibres' orientation angles were then analysed for each strip. The components of the fibres OT [25] for each strip were computed through orientation averages as follow:

$$a_{11} = \langle cos^2\theta_x \rangle$$

$$a_{22} = \langle cos^2\theta_y \rangle$$

$$a_{33} = \langle cos^2\theta_z \rangle$$

Resulting values of fibres OT components through the specimen thickness are reported in Figure 2.

µCT scans were performed on samples obtained at relevant positions along the specimen's gauge length, i.e. at its mid-length and at the end of the fillet radii, as shown and labelled in Figure 1.a. The nominal dimensions of the µCT-samples were 12mm x 4mm x 3.2 mm. A Waygate Technologies phoenix v|tome|x m CT scanner,

equipped with a dynamic 41|100 digital detector was used for the scans. The current and the acceleration voltage were set to 100 µA and 110 kV, respectively. The size of the voxel edge resulted to be 3.5 µm. Fibre orientation was evaluated from the µCT data by using the Fiber Composite Material Analysis (FCMA) module available in VGSTUDIO MAX, a Volume Graphic software intended to carry out analysis of the acquired volumes. A regular mesh, slicing the scanned volume of the samples in 33 cells across the thickness, allowed the average FO of each mesh cell to be automatically computed by the FCMA module. Results of the FO measurements are reported in Figure 2.a, Figure 2.b and Figure 2.c, in terms of the fibre OT's components through the specimens' thickness.

By comparing the FOD evaluated from µCT scanned samples (Figure 2.a, Figure 2.b and Figure 2.c), it is possible to observe a similar trend of the a_{11}, a_{22}, a_{33} OT components through the specimen's thickness, at any extraction location of the samples from the specimen. Moreover, the through the thickness FOD resulting from ellipsometry analyses (Figure 2.d) are in good agreement with those obtained from the µCT scans (Figure 2.a, Figure 2.b and Figure 2.c) up to 0.2 mm far from the outer surfaces of the specimen. Values of a_{33} were almost negligible, indicating a mainly planar FOD, in the *x*-*y* plane.

Two shell regions develop from the outer specimen's surfaces inward, having an extension of about 0.8 mm each. A relatively large core area was also observed, with the fibres nominally aligned at 90° respect to that in the shell region; this region was approximately 1 mm thick. However, in the core region fibres tend to display a certain degree of rotation in the x-y plane as suggested by non-zero values of the a_{12} OT component, evaluated from the CT scanned volumes analysis (Figure 2.a, Figure 2.b and Figure 2.c). The shell and the core areas showed a high degree of fibre alignment in the *x* and *y* direction, respectively, being the values of the maximum principal component of the fibre OT higher than 0.8 in both cases.

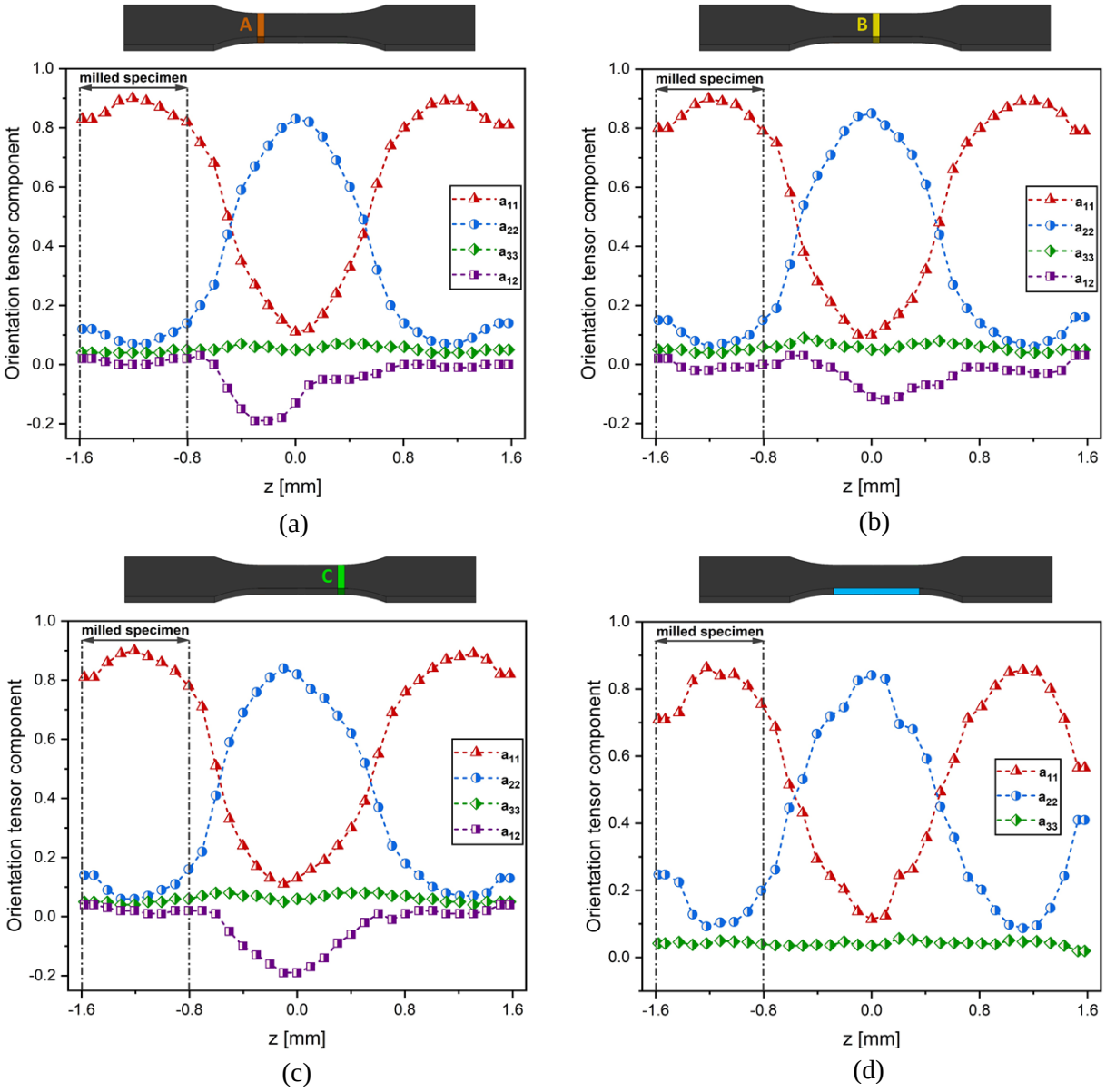

Figure 2 Averaged FOT components through the specimen thickness measured from µ-Ct analysis of a) Sample-A, b) Sample-B, c) Sample-C and d) measured by ellipsometry on the lateral surface of the specimen's gauge length The thickness of the milled specimen is also highlighted.

In contrast to what was found in [22] on a PA6 GF30, the transition from shell to core in PA66GF50 is smoother and occurs over a non-negligible region of the specimen thickness. This may be caused by the lower viscosity retained by the melt polymer due to the higher fibre content.

2.4 Results

The results of the quasi-static tensile tests carried out on the 0° and 90° full specimens are reported as stress-strain curves in Figure 3. An extended initial linear region featured the overall elasto-plastic response of the

material to the tensile load for both specimens' type. The Young's moduli were evaluated as recommended by the ISO 527-2 [10] standard and their average values are reported in Table 3. Tensile failure of the 0° full specimens occurred at a nominal stress of about 140 MPa and strain of 4%, while the 90° full specimens failed at a nominal stress of about 100 MPa and strain of about 3.2%. As expected, the 0° full specimens retained a higher tensile strength then their 90° counterparts.

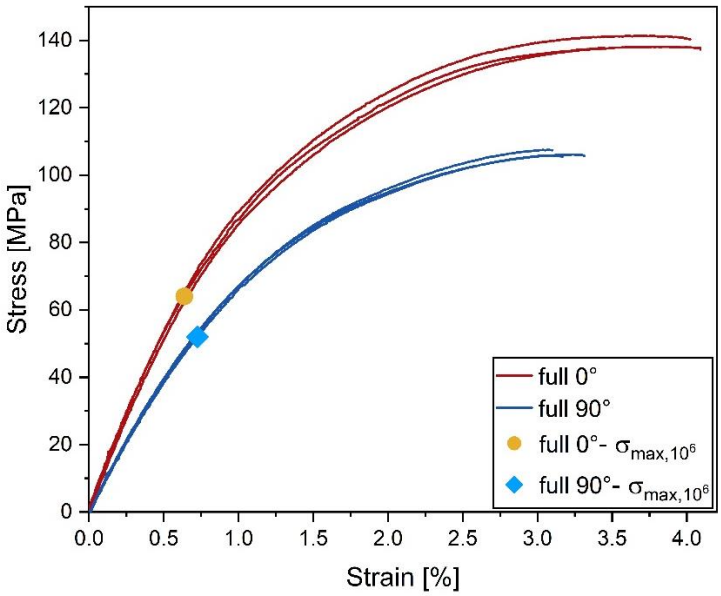

Figure 3 Stress-strain curves from tensile testing the full specimens. Markers indicate the stress considered for the numerical simulations.

The results of the fatigue tests, performed on the full and milled specimens, are plotted in Figure 4, where the maximum nominal stress applied, σ_{max}, is plotted against the cycles to failure N_f. S-N curves were obtained with the Basquin's equation $\sigma_{max} = \sigma_f{'}N^b$. The parameters of the interpolating curve are the fatigue strength exponent, b, and fatigue strength coefficient, $\sigma_f{'}$, whose values are listed in Table 1, together with values of the maximum applied nominal stress which would lead the specimens to fatigue failure at 10^6 loading cycles, $\sigma_{max,10^6}$, for each type of specimen and orientation.

Figure 4 highlights that the milled 0° specimens showed a higher number of cycles to failure than the 0° full ones. Conversely, the full 90° specimens outperformed their milled counterparts. This is due, as expected, to the higher degree of fibre alignment in the milled specimens. The slope of the S-N curves of milled specimens is slightly higher.

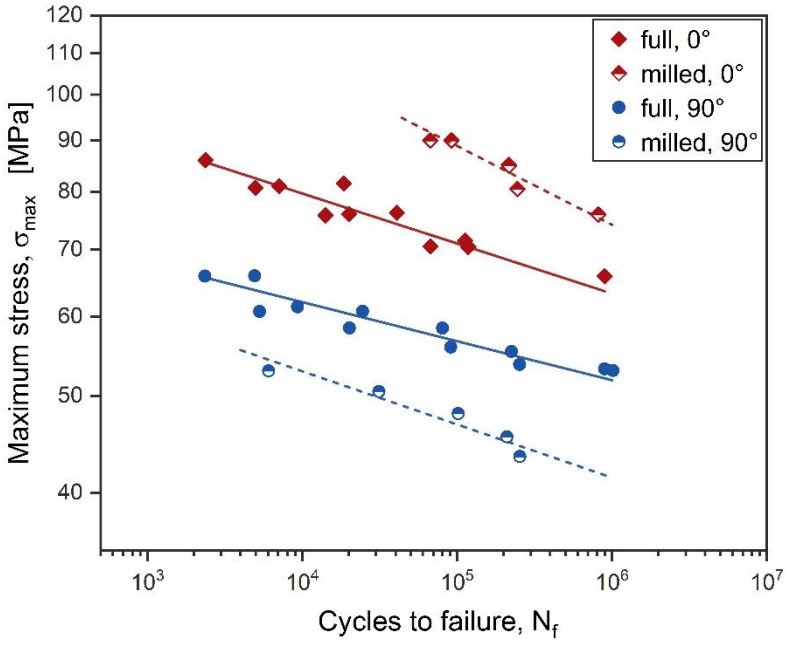

Figure 4 S-N curves of the milled specimens, superimposed to those of the full ones

Table 1. Full and milled specimens: values of the fitting parameters of the Basquin's equation and of the maximum applied nominal stress which would lead the specimens to fatigue failure at 10^6 loading cycles.

Specimen	σ_f' **[MPa]**	b	$\sigma_{max,10^6}$ **[MPa]**
0°			
Full	126.3	-0.050	64
Milled	219.9	-0.079	74
90°			
Full	88.9	-0.039	52
Milled	86.3	-0.053	42

Moreover, the fatigue fracture of the full specimens occurred almost in the middle of the gauge length, as shown in Figure 5.a and Figure 5.b, meaning that the fatigue failure was controlled by the local stresses acting in those regions. The propagation paths of the fractures were almost straight and perpendicular to the specimens' longitudinal axis, i.e. the loading direction. Conversely, the fatigue fracture of all the milled specimens was located in correspondence of the fillet radii, as shown in Figure 5.c and Figure 5.d. This occurrence could indicate that the crack initiation was dominated by the local stress concentration. This might also explain the observed higher slope of the S-N curves of the milled specimens. The full specimens thus

appear to be less notch sensitive than the milled ones. This may be caused by the different stiffnesses of two layers type (shell and core), which promote a stress redistribution through the specimens' thickness. The higher local value at the notch is thus less important than the higher global value in the mid-section due to the reduced area. A similar effect was observed in multidirectional hybrid laminates, for which the presence of laminae with different stiffness promotes ductility and reduced notch sensitivity [26].

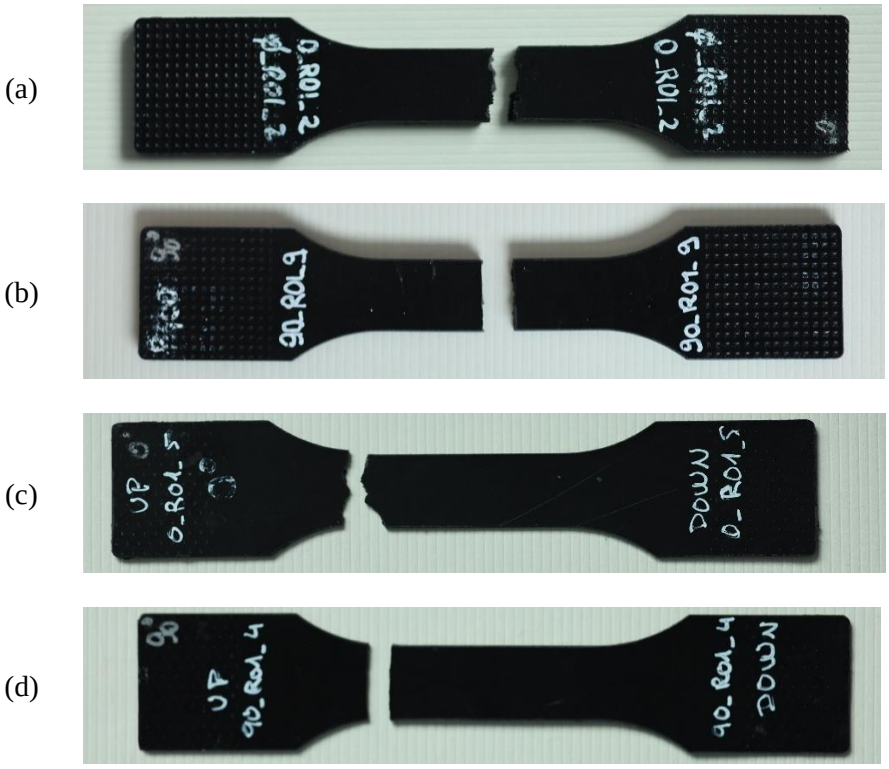

Figure 5 Images of the position and orientation of the fracture surfaces of the a) full 0° b) full 90° c) milled 0° d) milled90° specimens fatigue tested

3. Numerical analysis

3.1. Simulations settings

Numerical simulations were conducted to evaluate the stress distribution through the milled and full specimens' thicknesses, according to their local FO. Since the full specimens display a layered microstructure, it was reasonable to approximate them as composite laminates, with a non-uniform stress distribution through their thickness. Hence, two Finite Element Method (FEM) models of the full specimens were built, one for each main specimens' orientation (0° and 90° with respect to the plate's axis), to compute these local stress values.

Linear-elastic FE analysis were performed using the commercial software Simulia Abaqus 2018, developed by Dassault Systèmes [27]. Linear shell elements, with an average edge dimension of 0.5 mm, were used to build the mesh shown in Figure 6.

Figure 6 Finite element mesh used for structural analyses

The modelling strategy used to account for the effect of FOD upon the elasticity of the SFRPs assumes an equivalent laminate structure of the specimens and required a suitable homogenization technique. Therefore, the section of the specimens was modelled as a conventional shell composite layup. To each lamina a FO was assigned based on the measurements carried out on the µCT scanned sample-B, being representative of the FO at their failure location, i.e. the mid gauge-length, as previously discussed in section 2.4. Accordingly, the section of the model accommodated 33 laminae, since this was the number of cells through the specimens' thickness used to discretise the measured FOD. The fibre orientation data were then transferred to the structural mesh, in a layer-wise manner. This task was carried out by using the mapping tool of the Digimat 2019 software. Such tool allowed to consider the local FOD in each lamina. As a result, all the considered laminae were orthotropic, allowing to consider the contribution of all orientations in the 0°-180° range, weighted by the local FOD. A suitable homogenization technique was then required to evaluate the elastic constants of a unidirectional orthotropic lamina. To this purpose, a two-step Mori-Tanaka homogenization scheme, available in the Digimat software suite, was used. This technique is widely adopted for SFRPs [28-30].

Additional FEM models of the milled specimens were obtained from those of the full ones, by updating the thicknesses (from 3.2 mm to 0.8 mm) and the number of laminae according to the reduced thickness and the relative position. The assigned FO for this additional analysis were those evaluated from µCT of sample-B, representative of the stress distribution at the expected failure location, namely the mid gauge length, and those from µCT sample-A, representative of stress distribution at the actual failure location of the milled specimens, i.e. the end of the fillet radii, as discussed in section 2.4.

The properties of the fibres and matrix inputted to the homogenization scheme are reported in Table 2. The fibre aspect ratio is assumed equal to the typical average value of injection moulded SFRPs with this fibre content. The Young's modulus of the matrix was evaluated by applying an iterative Finite Element Analysis (FEA) based reverse engineering approach. As a first stage, FE simulations were run for the 0° and 90° full specimens by setting the initial guess value of the matrix Young's modulus equal to 2GPa. However, a slight discrepancy between the numerically obtained and experimentally evaluated longitudinal moduli was found for both the 0° and 90° specimens. Therefore, the same simulations were run iteratively, updating the value of the matrix Young's modulus at each iteration, until the numerical longitudinal moduli converged to the values of the experimental ones, within an error threshold of 10%. The values of the moduli thus obtained are reported in Table 3.

The FE models of the specimens were loaded and constrained to simulate the experimental test conditions. The clamping ends of the specimen were linked by a kinematic coupling to two reference points, in order to simulate the locking of the grips. The axial load exerted by the testing machine was applied to one of the two reference points, constraining all the degrees of freedom of the node but the axial displacement. All the degrees of freedom of the other reference point were constrained to be zero, simulating the fixed grip.

Table 2. Properties of the fibres and the matrix assumed in the homogenization schemes

Properties	**Matrix**	**Fibres**
Young's modulus (GPa)	2.35	72
Poisson's ratio	0.4	0.22
Aspect ratio	-	20
Volume fraction	0.69	0.31

Table 3. Longitudinal elastic modulus of full specimens with different orientations: measured (EXP) and evaluated numerically (FEA) In parentheses, the percentage difference between experimental and numerical results.

	Apparent longitudinal elastic modulus (GPa)	
Full specimen orientation	**EXP**	**FEA**
0°	11.1	11.43 (2.98)
90°	8.22	7.66 (7.3)

For each case, the applied load was determined as the load that would lead to failure the full and milled specimens at 10^6 cycles, respectively (see Figure 4). This was obtained by multiplying the nominal areas of the specimens' cross sections by $\sigma_{max,10^6}$, that is the maximum stress that would lead to failure the specimens at 10^6 cycles. The values of the $\sigma_{max,10^6}$ and of the loads applied in the numerical simulations, for each specimen's type and orientation, are reported in Table 4. The values of the applied nominal stress ($\sigma_{max,10^6}$) are also reported in Figure 3: it is shown how, at these stress levels, the specimens deviate very little from linearity, thus justifying the use of linear-elastic simulations.

Table 4. Values of the force, F_{max}, and the corresponding maximum nominal stress, $\sigma_{max,10^6}$, that would lead the full and milled specimens to failure at 10^6 loading cycles.

Specimen	**$\sigma_{max,10^6}$ (MPa)**	***F_{max}* *(kN)***
Full		
0°	64	2.41
90°	52	1.96
Milled		
0°	74	0.710
90°	42	0.398

The FE approach described is an established methodology for SFRP, and it was already used to evaluate different fatigue criteria for SFRP unnotched [12] and notched specimens [31].

3.2 Simulations results

The analysis of the stress distributions, obtained via numerical simulations, was performed considering the normal components of the plane stress tensor expressed in the local material reference frame, schematically shown in Figure 7, i.e. in a reference frame with the axes coinciding with the principal directions of the local fibre OT. These stress components are the longitudinal stress σ_1, that is the normal stress acting on a plane perpendicular to the first principal direction of the fibre OT, and the transverse stress σ_2, that is the normal stress acting on a plane perpendicular to the second principal direction of the fibre OT. Thanks to the discretisation of the specimens in 33 layers, retaining the local representative FO, the distribution of the local stresses through the thickness could be obtained.

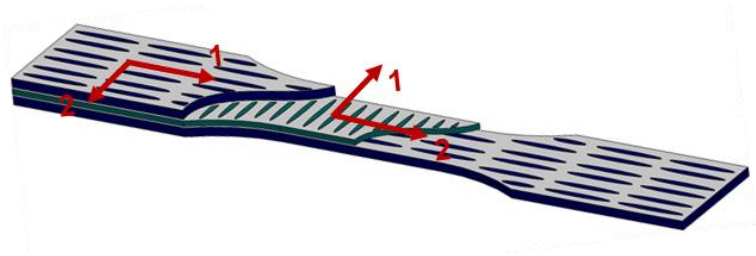

Figure 7 Local material reference frame used for the expression of the stress tensor on a schematic cut view of a full specimen

The values of the longitudinal and transverse stress components, evaluated at mid gauge length of the full 0° and 90° specimens, are reported in the graphs of Figure 8. As shown, the stresses varied significantly through the specimen's thickness because of the shell-core-shell microstructure of the specimens. Figure 8.a shows that in the shell layers of the 0° full specimens, where fibres are oriented parallel to the loading direction, the local values of the maximum component of the stress σ_1 ranges from about 70 to 90 MPa. In the core layer, where fibres are oriented perpendicularly to the loading direction, the maximum component of the stress σ_2 ranges from about 30 to 50 MPa.

The situation is almost symmetric for the 90°full specimens (Figure 8.b), where the maximum component of the stress in the shell layer is σ_2 and in the core layer is σ_1, being the fibre orientation opposite to that of the 0° full specimens. In this case, the maximum component of the stress, σ_2, in the shell layers displays nearly constant value of about 35 MPa. Whereas, in the core region, the local values of the maximum component of the stress, σ_1, range from about 70 to 100 MPa.

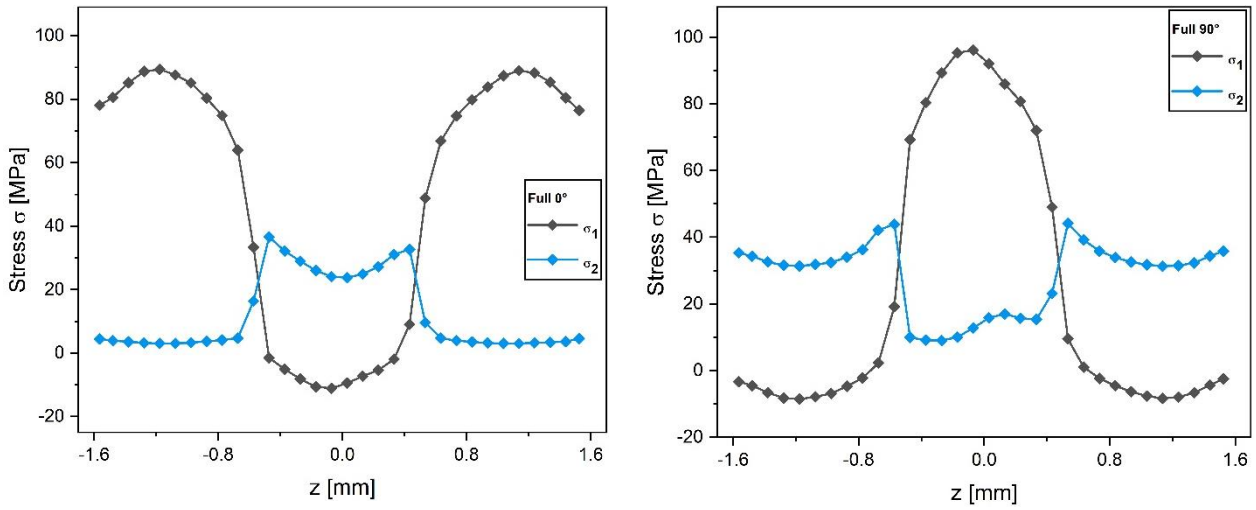

(a) (b)

Figure 8 Numerically obtained longitudinal and transversal stress distributions through the thickness evaluated at the mid gauge length of a) 0° and b) 90° full specimens

The values of the longitudinal and transverse stress components extracted at mid gauge length of the 0° and 90° milled specimens, retaining the FOD measured at the mid gauge length (Figure 2.b), are reported in orange in Figure 9.a and Figure 9.b, respectively.

However, as previously discussed in section 2.4, the failure of the milled specimens occurred at the end of the fillet radii. Therefore, the actual stress distribution that would lead them to fail at 10^6 cycles is more likely the one at the fillet's location rather than that at mid gauge length. The distributions of the stress components σ_1 and σ_2 in the fillet region of the specimens is in turn governed by the local FOD and by the local stress concentration. Their evaluation thence required the extraction of the stress values at the most stressed point of the fillet regions of the 0° and 90° milled specimens which retain the FOD measured at the fillet (Figure 2.a). These stress distributions are also reported in yellow in Figure 9.a and Figure 9.b, respectively.

Figure 9 shows that higher local values of the stress component σ_1 act in the fillet region of the 0° milled specimens, with a maximum value equal to 94 MPa. Conversely, similar local values of the stress component σ_2 act in the fillet region and at mid gauge length of the 90° milled specimens, with a maximum value equal to 47 MPa. This indicates that the same geometrical variation at the fillet induces different stress concentrations depending on the main orientation of the fibres. Considering the 90° milled specimens, the contribution of the stress concentration at fillet on the stress distribution is less significant than that of the 0° milled ones, as can

be observed from Figure 9.a-b. Nevertheless, consistent failures of the 90° milled specimens in the fillet region still shows that this stress concentration is not negligible.

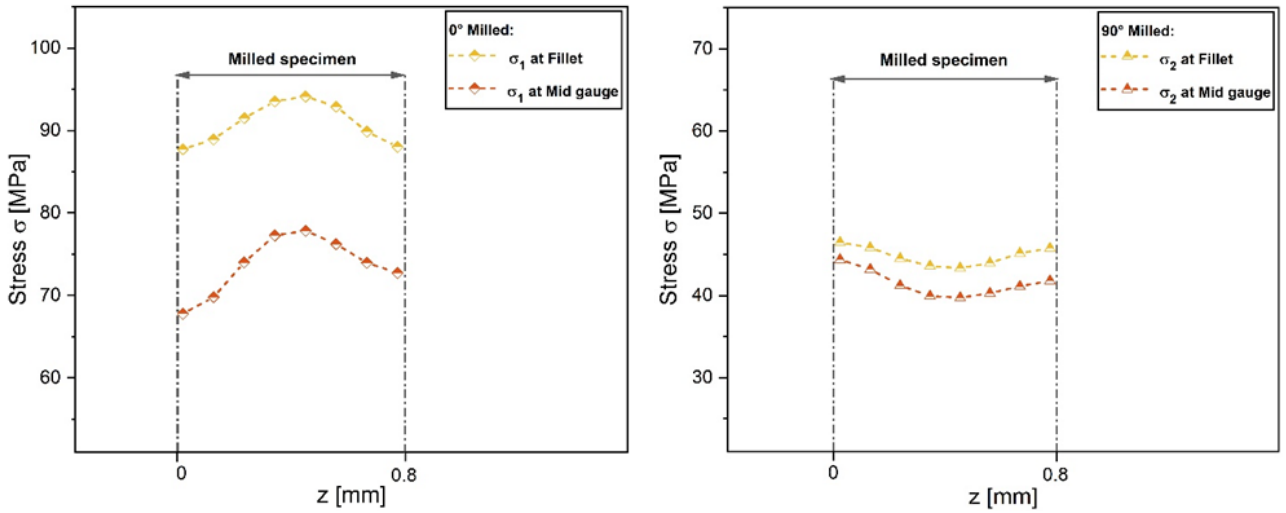

(a) (b)

Figure 9 Numerically obtained stress distributions through the thickness evaluated at the mid gauge length and at the fillet radii of a) 0° and b) 90° milled specimens

4. Discussion

4.1. Comparison of the results

In Figure 10, the FEA computed local stress distribution at the failure location (mid gauge length) under the action of the load that would lead the 0° and 90° full specimens to fatigue failure at 10^6 cycles are overlapped to those similarly obtained for the 0° and 90° milled specimens extracted at their actual failure location (end of the fillet region).

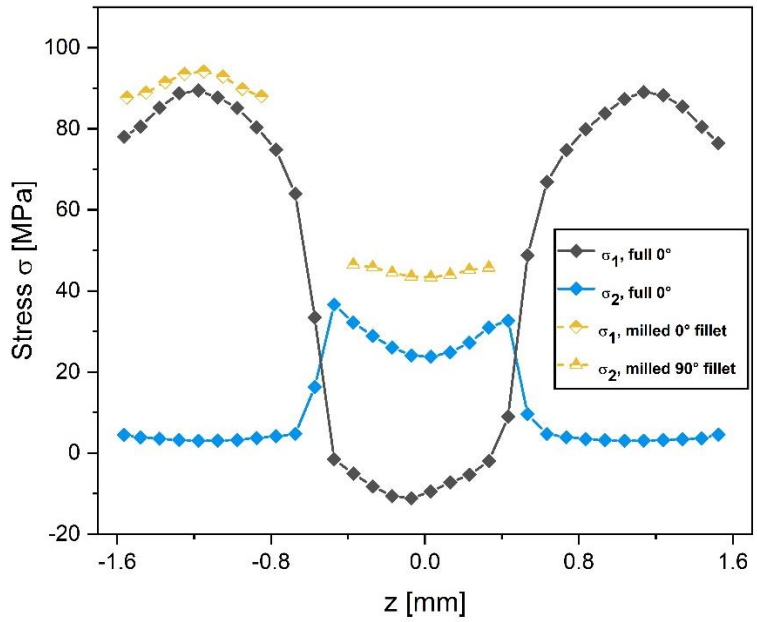

(a)

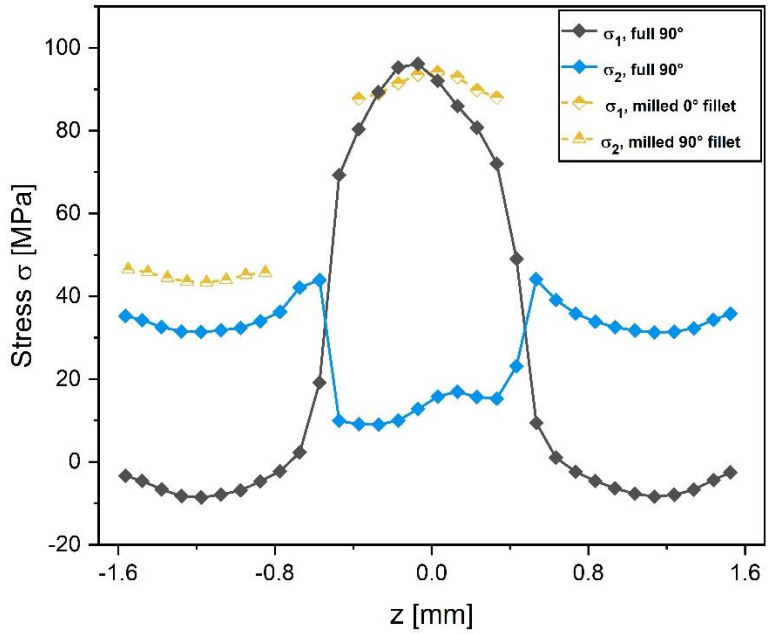

(b)

Figure 10 FEA computed local stress distributions that would lead the a) 0° and b) 90° full specimens to fatigue failure at 10^6 cycles, overlapped to those similarly obtained for the milled specimens at relevant location for the failure and to the experimentally evaluated fatigue strength of the milled specimens

The numerical simulations on the full specimens reproduce more accurately the stress distribution through the specimens' thickness at the peak load of the first half loading cycle. Considering the loss of stiffness phenomena occurring during the fatigue loading, the presented stress distribution for the full specimens does not necessarily remain constant during their fatigue life [7,11-12,32-34]. Conversely, the stress distribution

obtained for the milled specimens is believed to not vary significantly during the fatigue loading: these specimens feature a more coherent through-the-thickness fibre orientation distribution (see Figure 2); moreover, the fatigue tests were performed in load-controlled conditions, and thus any stress distribution predicted must always equilibrate the same outer load throughout the fatigue life of the specimens. Therefore, we considered the maximum value of the stress distribution in the milled specimens as the local fatigue strength of a material with a similar coherent orientation (prevailing 0° or prevailing 90°).

In both Figure 10.a and Figure 10.b, the stress in the 0° layers is very close or even above the 0° fatigue strength obtained from the milled specimens. Conversely, the 90° layers undergo a significantly lower stress than the 90° fatigue strength. This highlights that the 90° full specimens cannot be used to measure the real fatigue strength of a SFRP with a uniform 90° fibre orientation distribution. This issue is particularly important for multiscale model development, that often require the local fatigue strength of the material.

Moreover, the 0° layers were found to be at a more critical loading condition than the 90° layers in the first part of the specimens 'life. In-situ fatigue tests observed that damage occurs diffusively in all the layers of the specimens for SFRP materials [8]. This suggests that, while the damage evolution in SFRP is a complex phenomenon, and that continuous stress redistributions and stiffness losses occur in the layers, fatigue damage develops earlier in the 0° than in the 90° layers. The damage in the 0° layers causes their progressive loss of stiffness; since fatigue tests are load-controlled, this loss of stiffness likely causes a stress redistribution that increases the stress in the 90° layers. It is likely that this mechanism of redistribution of load shares is repeated until the final failure of the specimen or the end of the test.

An earlier damage development in the 0° layers than in the 90° layers is maybe unexpected, since the 0° layers are generally stronger. However, the 0° layers are also stiffer, and carry a higher portion of the applied load. The discontinuous nature of the SFRPs creates discontinuities in the stress fields, particularly at fibre ends [35]. Indeed, Rolland et al. [36] showed that fibre failure and debonding at fibre ends were not less frequent than fibre-matrix debonding along the lateral surfaces of the fibres.

4.2 On the use of the fatigue strength of the milled specimens as representative fatigue strength of the material

While it was suggested in the previous section that $\sigma_{max,10^6}$ of the full specimens does not provide a reliable indication of the fatigue strength of the actual material, it might also be questioned how representative the fatigue strengths of the milled specimens are. Two issues seem to play major roles in answering this question.

First of all, as already extensively discussed through the present work, the fatigue fracture location of all the milled specimens was in the correspondence of the fillet radii. Therefore, it is likely that the fatigue damage is anticipated by the stress concentration at the fillet location. This issue could be solved by designing specimens with a smaller stress concentration factor, knowing in advance that the milled specimens will be more susceptible to notches.

Another issue that makes it questionable the use of the fatigue strength of the milled specimens as a reliable indication of the strength of the material originates from the possibility that the milling process introduced some damage on the machined surface of the milled specimens, creating preferential sites for the onset of cracks. This may cause early failure of the specimens, and consequently lead to the underestimation of the true local strength of the milled specimens. To evaluate this possibility, the machined surfaces of the milled specimens were analysed with a Scanning Electron Microscope (SEM) to detect signs of damage and compared them with the as-moulded surfaces. The observed specimens' surfaces underwent a gold sputtering prior to scan, to enhance the quality of the images. The SEM images of the machined and of the as-moulded surfaces of fatigue tested specimens are shown in Figure 11.

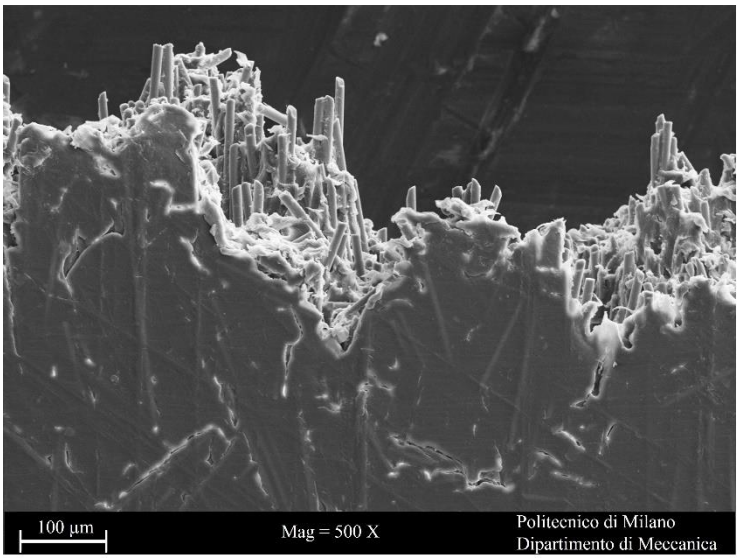

(a)

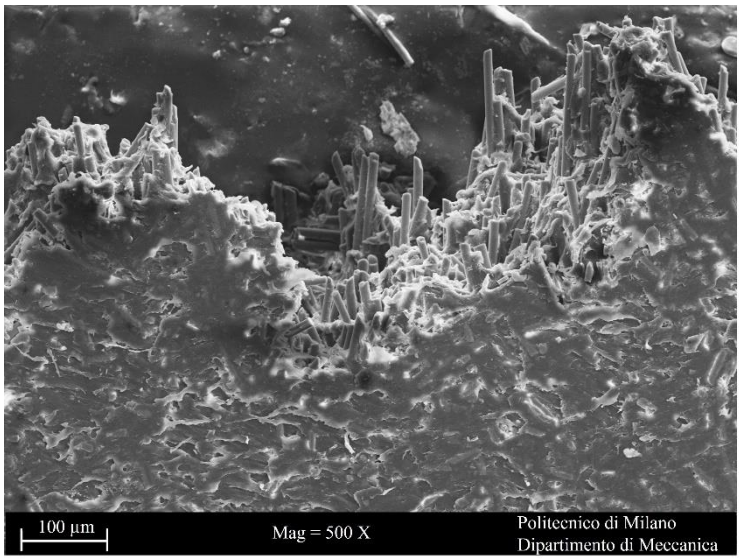

(b)

Figure 11 SEM images of the side surfaces of the milled specimens, in particular a) the as-moulded surface and b) the machined surface

The as-moulded face, shown in Figure 11.a, displays a very smooth and regular surface where even some shallow fibres, emerging from the surface, are visible. Microcracks, compatible with the fatigue damaging mechanism of the investigated material [37], can be also spotted on the surface as the result of localized damage caused by fatigue testing of the specimen.

In contrast, on the machined surface, shown in Figure 11.b, it is possible to see regions where the polyamide matrix is spread over the surface, with the formation of wrinkles. This could be the consequence of the combined effect of the mechanical action of the milling tool and of the heat generated by the milling process,

that caused the melting of the matrix material. No fibres pultruded from the surface were observed, that could have been an indication of the damaging caused by the milling.

In any case, no clear evidence of damaging could be detected by this surface analysis, although the aspect of the machined surface is very different from the as-moulded one. Therefore, additional surface roughness measurements were performed on a milled specimen and on a full specimen, on their machined and the as-moulded surfaces, respectively. The measurements were performed according to the ISO 4288:1998 [38] standard, using a Mahr PGK contact profilometer. The radius of the stylus was 2 µm. For every surface type, the measurements were performed over three paths inclined at 0°, 90° and 45° with respect to the specimens' axis. The average surface roughness, R_a, was taken as the average value of the three measurements along the prescribed paths. The average R_a values were 2.5 µm and 0.3 µm for the machined and as-moulded surfaces, respectively. These measurements show that, as expected, the machined surfaces are rougher than their as-moulded counterparts. A higher surface roughness could indeed lower the fatigue resistance of the milled specimens for both the orientations considered (0° and 90°) [39].

Due to these two issues, the experimentally observed fatigue strengths of the milled specimens, might be considered as a lower bound for the strength of a material with highly oriented fibres. Therefore, further work should focus on the design and preparation of specimens more suitable for this type of investigation, like specimens with optimized shape of the transitions from gauge section to the clamping end region, to minimize stress concentrations, extracted from plates with uniform through the thickness fibre orientation (unidirectional plates) [40].

A further development of this work can thus be the search for alternative methods of obtaining shell-only specimens to test under fatigue condition. A possible solution could be to injection mould specimens with different thickness, which usually implies a different core thickness [41]. It would be possible in this way to extrapolate the strength of a material with null core thickness by evaluating the strength of each specimen and by interpolating the results. However, De Monte et al. [41] showed that specimens with 1 mm thickness still displayed a layered microstructure. Therefore, a shell-only injection moulded specimen may need to be significantly thinner than the 0.8 mm milled specimens analysed in this work. This poses both additional technological challenges and doubts on the influence of a size effect of the measured mechanical properties of

such thin specimens. More recently, Van Roo et al. [40] were able to injection mould 2 mm unidirectional SFRPs specimens. The authors, however, had to design a specific injection moulding tool, with an enlarged inlet, specifically for this purpose. This was the result of a design and optimisation procedure involving process simulations. Injection moulding shell-only specimens is thus still a complex procedure, that requires careful specimens and tool design. Finally, aligned discontinuous composites may be obtained through other methods that do not involve injection moulding [42].

5. Conclusions

This work presented the results of experiments conducted on full specimens, cut-out from injection moulded plates at 0° and 90° with respect to the main flow direction, and on similar specimens that were machined to preserve only one shell layer. The experimental results were compared with the results of a FE analyses, which accounted for the actual fibre orientation at the failure location of each specimen configuration, and for the local material's properties, defined according to the fibre orientation distribution.

It was experimentally confirmed that the milled 0° specimens have a superior fatigue behaviour than the 0° full ones. This is the consequence of the high alignment of the fibres along the specimen's axis in the milled 0° specimens, whereas the full specimens have a quite thick core region where fibre are oriented transversally to the specimen's axis. For the opposite reason, the milled 90° specimens displayed inferior fatigue performance than their full counterparts. While these were two expected results, they allowed a deeper analysis on the failure mechanisms of SFRPs, supported by numerical simulations, to be carried out.

In particular, the comparison between the FEA obtained local stress distributions for the full specimens and the fatigue strength of the milled specimens revealed that, for both specimens' orientations, the fatigue damage is more likely to be initiated in the layers with fibres oriented with the specimen's axis, i.e. with the loading direction. Damage then likely diffuses to the other layers due to the local loss of stiffness. This observation led to an important conclusion: the 90° full specimens, with a non-negligible core thickness, do not allow the fatigue strength of a material with fibres perpendicular to the load to be evaluated.

Finally, it is considered if the milled specimens could lead to a reliable estimation of the fatigue strength of a highly oriented material. The failure of these milled specimens in correspondence of the fillet radii and the

potential detrimental effect introduced by the milling process on the side surface of the specimens, seem to be against such claim. However, these specimens clearly provide a lower bound estimate of the fatigue strength of a highly aligned short fibre reinforced material. Therefore, testing highly oriented milled specimens, together with the full ones, can still provide more useful information than testing the full specimens alone and ignoring their layered microstructure. This is of particular importance when the local fatigue strength of the material is required for TPM purposes.

Acknowledgements

The authors wish to thank P. Barriga Ruiz and D. Moretti for their help in conducting the tests, R. Galeazzi and C. Ghilardi for their support to the simulations. Smart NDT company, L. Tentorio and L.Lorenzi are gratefully acknowledged for carrying out the µ-CT scans and supporting the fibre orientation analysis.

References

[1] S. Mortazavian and A. Fatemi, "Fatigue behavior and modeling of short fiber reinforced polymer composites: A literature review". *Int J Fatigue,*70:297-321, 2015.

[2] J. J. Horst and J. L. Spoormaker, "Mechanism of fatigue in short glass fiber reinforced polyamide 6". *Polym Eng Sci*, 36(22):2718-2726, 1996.

[3] A. Zago and G. S. Springer, "Constant Amplitude Fatigue of Short Glass and Carbon Fiber Reinforced Thermoplastics". *J Reinf Plast Compos,* 20:564-595, 2001.

[4] Y. Zhou and P. K. Mallick, "Fatigue performance of an injection-molded short E-glass fiber-reinforced polyamide 6,6. I. Effects of orientation, holes, and weld line". *Polym Composite,* 27(2):230-237, 2006.

[5] K. Friedrich, "Microstructural efficiency and fracture toughness of short fiber/thermoplastic matrix composites". *Compos Sci Technol*, 22(1):43-74, 1985.

[6] J. Brunbauer, A. Moesenbacher, C. Guster, G. Pinter, "Fundamental influences on quasistatic and cyclic material behavior of short glass fiber reinforced polyamide illustrated on micorscopic scale". *Journal of Applied Polymer Science,* 131,40842, 2014.

[7] M. Arif, N. Sainter, F. Meraghni, J. Fitoussi, Y. Chemisky, G. Robert, "Multiscale fatigue damage characterization in short glass fiber reinforced plyamide-66". *Compos Part B-Eng*, 61:55-65, 2014.

[8] H. Rolland, N. Saintier, I. Raphael, N. Lenoir, A. King, G. Robert, "Fatigue damage mechanisms of short fiber reinforced PA66 as observed by in-situ synchrotron X-ray microtomography". *Composites Part B: Engineering*, 143:217-229,2018.

[9] A. Bernasconi, P. Davoli, A. Basile, A. Filippi, "Effect of fibre orientation on the fatigue behaviour of a short glass fibre reinforced polyamide-6". *Int J Fatigue,* 29(2):199-208, 2007.

[10] *ISO 527-2. Plastics - Determination of tensile properties - Part 2: Test conditions for moulding and extrusion plastics,* International Organization For Standards, 2012.

[11] M. De Monte, E. Moosbrugger, M. Quaresimin, "Influence of temperature and thickness on the off-axis behaviour of short glass fibre reinforced polyamide 6.6 – cyclic loading". *Compos Part A - Appl S,* 41(10):1368-1379, 2010.

[12] B. Klimkeit, Y. Nadot, S. Castagnet, C. Nadot-Martin, C. Dumas, S. Bergamo, C. Sonsino, A. Bueter, "Multiaxial fatigue life assessment for reinforced polymers". *International Journal of Fatigue,* 33:766-780, 2011.

[13] A. Moesenbacher, J. Brunbauer, P. Pichler, C. Guster, G. Pinter, "Modelling and validation of fat5igue life calculation method for short fibre reinforced injection moulded parts". In *ECCM 16,* Seville, 2014.

[14] C. Guster, G. Pinter, A. Mösenbacher, Eichlseder, "Evaluation of a simulation process for fatigue life calculation of short fibre reinforced plastic components". *Procedia Eng,* 10:2104-2109, 2011.

[15] A. Launay, M. Maitournam, Y. Marco, I. Raoult, "Multiaxial fatigue models for short glass fiber reinforced polyamide - Part I: Nonlinear anisotropic constitutive behavior for cyclic response". *International Journal of Fatigue,* 47:382-389, 2013.

[16] A. Launay, M. Maitournam, Y. Marco, I. Raoult, "Multiaxial fatigue models for short glass fibre reinforced polyamide. Part II: Fatigue life estimation". *International Journal of Fatigue,* 47:390-406, 2013.

[17] G. Stadler, A. Primetzhofer, G. Pinter, F. Grün, "Evaluation and consideration of local specimen material properties in lifetime prediction of short fiber-reinforced PA6T/6I". *Fatigue Fract Eng Mater Struct,* 45(4):980- 990, 2022.

[18] S. Mortazavian and A. Fatemi, "Fatigue behavior and modeling of short fiber reinforced polymer composites including anisotropy and temperature effects". *Int J Fatigue,* 77:12-27, 2015.

[19] S. Mortazavian and A. Fatemi, "Effects of fiber orientation and anisotropy on tensile strength and elastic modulus of short fiber reinforced polymer composites". *Comp PartB Eng,* 72:116-129, 2015.

[20] A. Jain, J. Veas, S. Straesser, W. Van Paepegem, I. Verpoest, S. Lomov, "The Master SN curve approach - A hybrid multi-scale fatigue simulation of short fiber reinforced composites". *Composites: Part A, 91(2):510-518,* 2016.

[21] A. Jain, "On the multi-axial fatigue modelling of short fibre reinforced composites: Extensions to the Master SN curve approach". *Int J Fatigue,145,* 106106, 2021.

[22] A. Bernasconi, A. Cavallaro, E. Conrado, P. Hine, "Experimental investigation on the true local fatigue strength of shell-core layered, injection moulded specimens of short fibre reinforced polyamide". In *ECCM 18.*

[23] ASTM D3479/3479M. *Standard Test Method for Tension-Tension Fatigue of Polymer Matrix composite Materials*. American Society for Testing and Materials, 2002.

[24] P. J. Hine, N. Davidson, R. A. Duckett, I. M. Ward, "Measuring the fibre orientation and modelling the elastic properties of injection moulded long glass fibre reinforced nylon". *Compos Sci Technol,* 53(2): 125-131, 1995.

[25] S.G. Advani and I. C. Tucker, "The Use of Tensors to Describe and Predict Fiber Orientation in Short Fiber Composites". *J Rheology,* 31:51-784, 1987.

[26] G. Czél, T. Rev, M. Jalalvand, M. Fotouhi et al. "Pseudo-ductility and reduced notch sensitivity in multi-directional all-carbon/epoxy thin-ply hybrid composites". *Composites Part A: Applied Science and Manufacturing*, 104:151-164, 2018.

[27] Dassault Systemes, Abaqus v2018 Manual, 2018.

[28] A. Jain, Y. Abdin, W. Van Paepegem, I. Verpoest, S.V. Lomov,"Effective anisotropic stiffness of inclusions with debonded interface for Eshelby-based models". *Composite Structures*, 131:692-706, 2015.

[29] A. Jain, S.V. Lomov, Y. Abdin, I. Verpoest, W. Van Paepegem, "Pseudo-grain discretization and full Mori Tanaka formulation for random heterogeneous media: Predictive abilities for stresses in individual inclusions and the matrix". *Composites Science and Technology*, 87:86-93, 2013.

[30] A. Jain, "Micro and mesomechanics of fibre reinforced composites using mean field homogenization formulations: A review". *Materials Today Communications*, 21,100552, 2019.

[31] S. Castagnet, C. Nadot-Martin, N. Fouchier, E. Conrado, A. Bernasconi, “Fatigue life assessment in notched injection-molded specimens of a short-glass fiber reinforced Polyamide 6 with different injection gate locations”, *International Journal of Fatigue*, 143, 105968, 2021.

[32] M. Arif, F. Meraghni, Y. Chemisky, N. Despringre, G. Robert, “In situ damage mechanisms investigation of PA66/GF30 composite: Effect of relative humidity”. *Composite Part B: Engineering*, 58:487-495, 2014.

[33] B. Klimkeit, S. Castagnet, Y. Nadot, A. El Habib, G. Benoit, S. Bergamo, et al. “Fatigue damage mechanisms in short fiber reinforced PBT+PET GF30”. *Mater Sci Eng A*, 528: 1577-1588,2011.

[34] A. Jain, W. Van Paepegem, I. Verpoest, S. V. Lomov, “A statistical treatment of the loss of stiffness during cyclic loading for short fiber reinforced injection molded composites”. *Composites Part B: Engineering*, 103:40-50, 2016.

[35] J. Henry, S. Pimenta, "Semi-analytical simulation of aligned discontinuous composites". *Composites Science and Technology*, 144:230-244, 2017.

[36] H. Rolland, N. Saintier, N. Lenoir, A. King, G. Robert, "Fatigue mechanisms description in short glass fibre reinforced thermoplastic by microtomographic observations". *Procedia Structural Integrity*, 2:301-308,2016.

[37] J. J. Horst and J. L. Spoormaker, “Fatigue fracture mechanisms and fractography of short-glass fibre-reinforced polyamide 6”. *Journal of Material Science*, 32:3641-3651, 1997.

[38] *ISO 4288:1998. Geometric Product Specification (GPS)-Surface texture- Profile method: Rules and procedures for the assessment of surface texture*, International Organization For Standards, 1998.

[39] C. Bauer, M. Magin, T. Schalk, “Influence of the Surface Finish on Fatigue Properties of SFRP under Mechanical and Environmental Loads”. In *International Conference on Fatigue of Composites, Paris, 2015*.

[40] T. van Roo, “Optimized injection moulding tool facilitates direction-dependent characteristic value determination and reliable component design”. *Published online: https://2018.lbf-jahresbericht.de/en/services/project-overview/polymer-technology/optimized-injection-moulding-tool-*

facilitates-direction-dependent-characteristic-value-determination-and-reliable-component-design/, Annual report 2018, Fraunhofer LBF, Apr. 2019.

[41] M. De Monte, E. Moosbrugger, M. Quaresimin, "Influence of temperature and thickness on the off-axis behaviour of short glass fibre reinforced polyamide 6.6 - Quasi-static loading". *Composites Part A: Applied Science and Manufacturing*, 41 (7):859-871, 2010.

[42] H. Yu, K.D. Potter, M.R. Wisnom, "A novel manufacturing method for aligned discontinuous fibre composites (High Performance-Discontinuous Fibre method)". *Composites Part A: Applied Science and Manufacturing*, 65: 175-185, 2014.